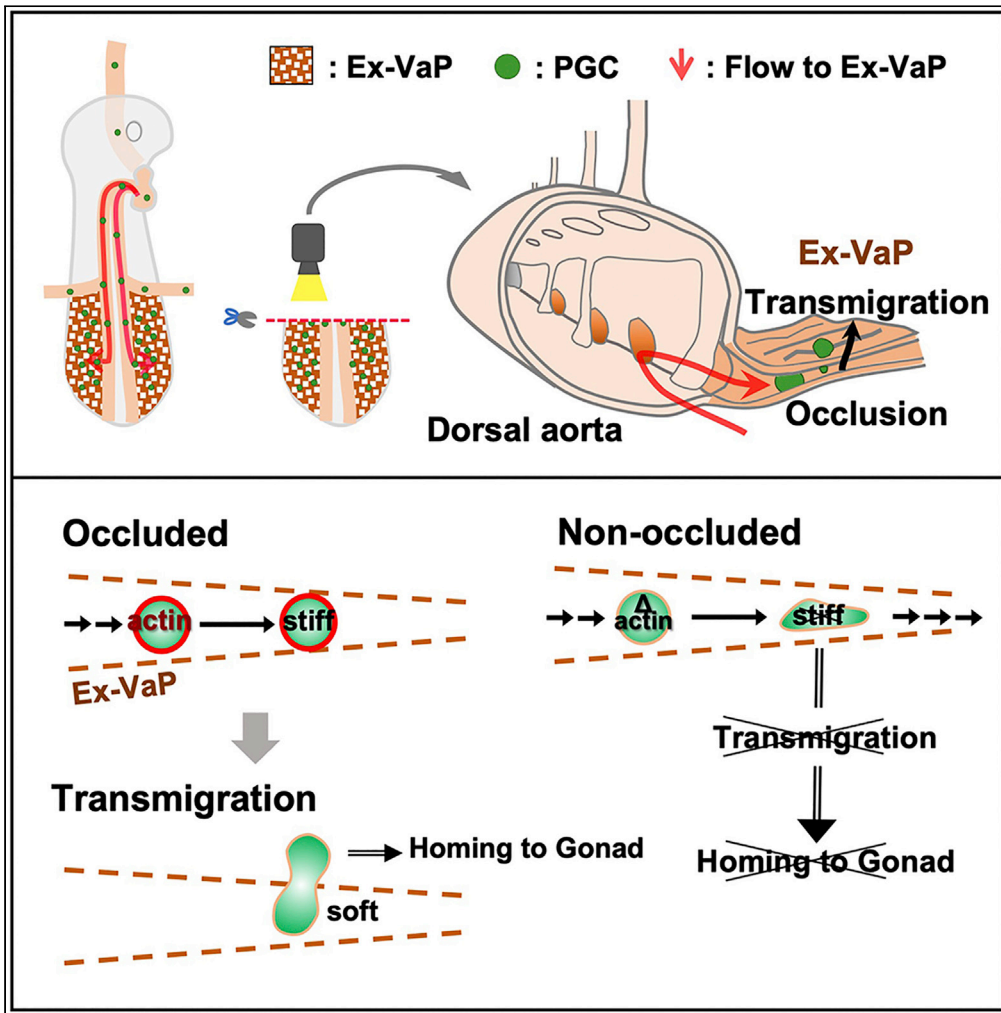# iScience

Article

Stiffness of primordial germ cells is required for their extravasation in avian embryos

Daisuke Saito,
Ryosuke
Tadokoro, Arata
Nagasaka, ...,
Takaki Miyata, Koji
Tamura, Yoshiko
Takahashi

saito.daisuke.036@m.
kyushu-u.ac.jp (D.S.)
yotayota@develop.zool.
kyoto-u.ac.jp (Y.T.)

Highlights

PGC arrest at Ex-VaP is
predominantly governed
by occlusion

The circulating PGCs are
highly stiff endorsed by
cortical actin

Actin-mediated stiffness
of PGCs is critical for the
occlusion

PGCs reset their stiffness
for transmigration

Article

Stiffness of primordial germ cells is required for their extravasation in avian embryos

Daisuke Saito,[1,2,3,11,*] Ryosuke Tadokoro,[4,5] Arata Nagasaka,[6,7] Daisuke Yoshino,[1,8] Takayuki Teramoto,[3] Kanta Mizumoto,[4] Kenichi Funamoto,[9] Hinako Kidokoro,[2,10] Takaki Miyata,[7] Koji Tamura,[2] and Yoshiko Takahashi[4,*]

SUMMARY

Unlike mammals, primordial germ cells (PGCs) in avian early embryos exploit blood circulation to translocate to the somatic gonadal primordium, but how circulating PGCs undergo extravasation remains elusive. We demonstrate with single-cell level live-imaging analyses that the PGCs are arrested at a specific site in the capillary plexus, which is predominantly governed by occlusion at a narrow path in the vasculature. The occlusion is enabled by a heightened stiffness of the PGCs mediated by actin polymerization. Following the occlusion, PGCs reset their stiffness to soften in order to squeeze through the endothelial lining as they transmigrate. Our discovery also provides a model for the understanding of metastasizing cancer extravasation occurring mainly by occlusion.

INTRODUCTION

During early embryogenesis in vertebrates, primordial germ cells (PGCs) emerge in an extraembryonic region and translocate intraembryonically to the gonadal primordia (developing gonad).[1,2] A failure of the PGCs' translocation causes sterility.[3]

The modes of PGCs' translocation are divergent among species. Unlike mammals and teleost fish in which PGCs migrate within stroma/tissues to home to the gonadal primordia, PGCs in avian (bird) embryos exploit blood circulation to translocate to a specific region, where cells undergo extravasation followed by an intra-stroma migration to home to the gonad.[4,5] Avian PGCs emerge in the anterior-most extraembryonic region called germinal crescent at Hamburger & Hamilton (HH) stage 8–10,[6,7] and later they are integrated into blood circulation at HH12. By HH16, PGCs accumulate in a specific region of the capillary bed (vascular plexus) in the splanchnic lateral plate near the gonadal primordia.[8] At this site, PGCs are arrested in the vasculature followed by transmigration through the endothelial lining to exit the vasculature (extravasation) and invade the mesenteric primordium.[8] However, it remains largely unknown how the intravascular arrest and transmigration at the specific site of vasculature are regulated.

We here demonstrate with live imaging at a single-cell level *in vivo* that the arrest of PGCs is predominantly governed by occlusion at a narrow path in the capillary bed. In addition, this occlusion is enabled by a heightened stiffness of the PGCs, revealed by atomic force microscopy (AFM) indentation assays. The PGCs' stiffness is regulated by cortical actin polymerization: inhibition of the actin function causes a failure of not only the PGC occlusion in the capillary bed but also colonization in the gonads at later stages. Following the occlusion in the vascular bed, PGCs reset their stiffness to soften in order to squeeze through the endothelial lining as they transmigrate. The regulation of F-actin-mediated stiffness found in this study might be shared by metastasizing cancer cells that also undergo an intravascular arrest prior to extravasation.

RESULTS

Intravascular PGCs accumulate and extravasate in Ex-VaP

To visualize intravascular distribution of PGCs in early embryos, we have conducted either an infusion with fluorescent ink to label PGC-contained circulating cells and immune-staining with DEAD-box helicase 4 (DDX4) for PGCs or co-staining with DDX4 and QH1 (vascular marker for quail). In this study, chicken embryos are used except for experiments with QH1 staining which is available only with quail embryos. Quail embryos are also staged according to HH-staging system showing equivalent stages with chickens. These

[1]Frontier Research Institute for Interdisciplinary Sciences, Tohoku University, Sendai, Miyagi 980-8578, Japan

[2]Department of Ecological Developmental Adaptability Life Sciences, Graduate School of Life Sciences, Tohoku University, Sendai, Miyagi 980-8578, Japan

[3]Department of Biology, Faculty of Science, Kyushu University, Fukuoka, Fukuoka 819-0395, Japan

[4]Department of Zoology, Graduate School of Science, Kyoto University, Kyoto, Kyoto 606-8502, Japan

[5]Department of Bioscience, Okayama University of Science, Okayama, Okayama 700-0005, Japan

[6]Division of Histology, Meikai University School of Dentistry, Sakado, Saitama 350-0283, Japan

[7]Department of Anatomy and Cell Biology, Nagoya University Graduate School of Medicine, Nagoya, Aichi 466-8550, Japan

[8]Institute of Engineering, Tokyo University of Agriculture and Technology, Koganei, Tokyo 184-8588, Japan

[9]Institute of Fluid Science, Tohoku University, Sendai, Miyagi 980-8577, Japan

[10]Organization for Research Initiatives and Development, Doshisha University, Kyotanabe, Kyoto 610-0394, Japan

[11]Lead contact

*Correspondence:
saito.daisuke.036@m.kyushu-u.ac.jp (D.S.),
yotayota@develop.zool.kyoto-u.ac.jp (Y.T.)
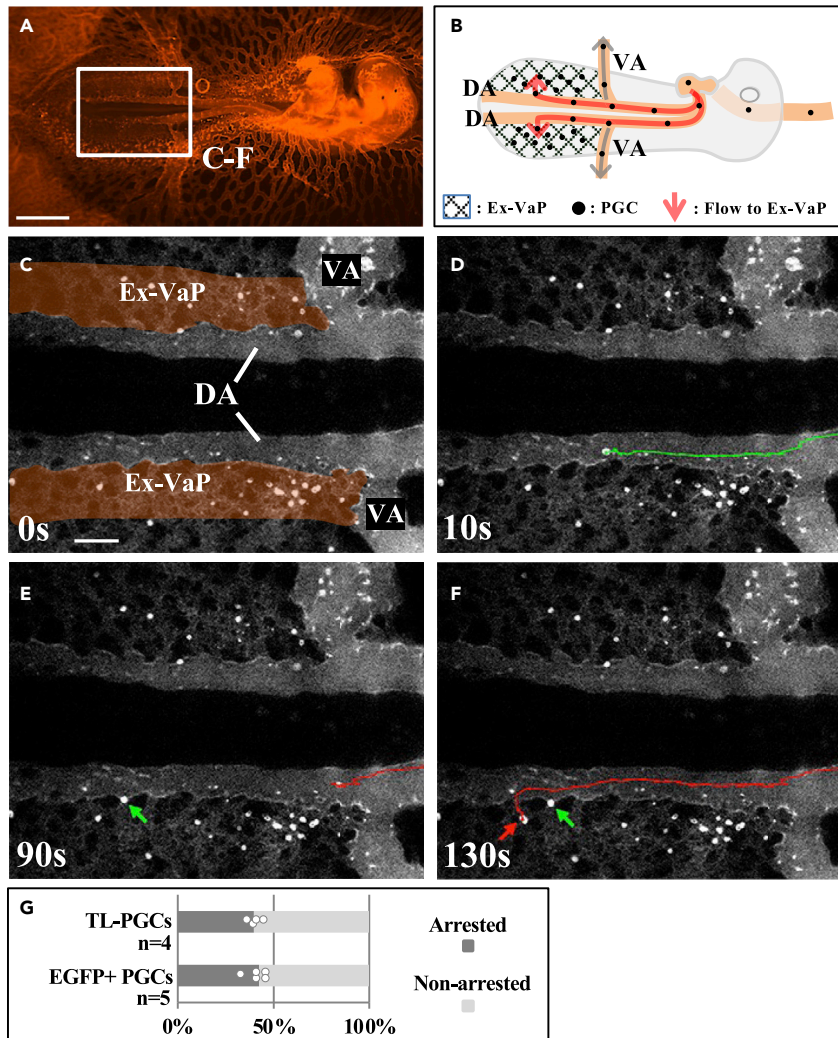https://doi.org/10.1016/j.isci.2022.105629

Figure 1. Circulating PGCs are arrested in Ex-VaP of HH15 chick embryo

(A) Ventral view infused with fluorescent ink.

(B) Diagram of circulation and arrest of PGCs in Ex-VaP.

(C–F) Motion captures at 0s, 10s, 90s, and 130s from the movie corresponding to the square in A (Video S1) show that some of TL-labeled endogenous PGCs (bright spots) circulating in the dorsal aortae are arrested in Ex-VaP (arrows). Green and red lines are tracks of two different PGCs.

(G) Quantification of arrested PGCs. TL-labeled endogenous PGCs (301 cells; 4 embryos), and back-infused EGFP + PGCs (527 cells; 5 embryos) were assessed in Ex-VaP. DA, dorsal aorta; VA, vitelline artery. Scale bars: 1,000 μm in A, 200 μm in C. Please see also Figures S1 and S2; Videos S1 and S2.

analyses demonstrate that PGCs are widely distributed in blood vessels at HH12 including extraembryonic vasculature (Figures 1 and S1). By HH16, they are confined to a specific region of the embryonic capillary bed (vascular plexus) near the pair of presumptive gonads, which are located posteriorly to the vitelline arteries (VAs) running mediolaterally at the level of the 20th somite (Figures 1 and S1), consistent with previous reports by electron microscopic examination.[8] We have also confirmed that the intravascularly trapped/arrested PGCs subsequently undergo transmigration to invade the splanchnic lateral plate (mesenteric primordium) and ultimately home to the gonad primordia. In this study, the region of vascular plexus accommodating extravasating PGCs is designated as Ex-VaP (extravasation vascular plexus).

Circulating PGCs are arrested in Ex-VaP

A two-dimensional (2D) flat structure of early chicken embryos facilitates high-speed recording of intravascularly labeled PGCs to visualize their arrest in Ex-VaP at a single-cell level. At HH15, tomato

lectin-conjugated fluorescein isothiocyanate (FITC)-labeled PGCs (TL-PGCs) in the pair of dorsal aortae (DA) move intermittently obeying the rhythm of heartbeat (Figure 1 and Video S1). Whereas the majority of PGCs in DA turn into VAs at the 20th somite level and quickly flow out from embryo-proper, some PGCs keep circulating down posteriorly in DA and finally turn laterally into Ex-VaP (Figure 1 and Video S1). Because Ex-VaP is composed of meshwork-like narrow paths of vasculature, the velocity of PGC circulation is much lower than that in DA (150 μm/s and 300 μm/s in Ex-VaP and DA, respectively). Approximately 40% of the Ex-VaP-entering PGCs are arrested (Figure 1 and Video S1), whereas the rest of the cells escape from the arrest and flow away toward extraembryonic vasculature, from which they probably circulate back into embryo-proper. The patterns of the circulation and arrest of TL-PGCs are comparable with those with CAGGS:EGFP-expressing PGCs (arresting rate: 40.9 ± 4.5%), which were stably transfected in vitro by using transposon Tol2 system and back-transplanted/infused into host embryos (Figures 1G and S2; Video S2).[9,10]

The majority of PGCs are occluded at constriction points in Ex-VaP

A 3D-reconstructed image of vasculature at HH15 demonstrates a fine structure of DA through which PGCs enter Ex-VaP (Figure S3). In the ventrolateral wall of DA, multiple passage branches (connection ports) connecting to Ex-VaP are observed, which are often associated with a pillar-like structure, which might lead PGCs into Ex-VaP (Figure S3). Ports connecting to inter-somitic (intersegmental) vessels are also seen in the dorsal side of DA. The 3D-reconstructed vasculature has also revealed an intricate mesh-like structure of Ex-VaP that contains the smallest (narrowest) paths of 10 μm wide (Figures 2A–2D and S4), where PGCs are frequently occluded (65.7%; Figures 2C–2E, 2H, and S4). These occluded sites are designated as constriction points.

To more precisely identify the distinguishing features of arrested PGCs in Ex-VaP, we have conducted high-resolution live-imaging microscopy at the single-cell level and observed two more types of PGC's arrest in addition to the occlusion type: one is an adhesion type in which PGCs are simply adhered to the endothelial lining regardless of the constriction point (29.8%) (Figures 2F, 2H, and S4; Video S3) and the other type is a thrombus-mediated PGC arrest (4.5%), where single PGC is encapsuled by multiple blood cells (BCs; erythrocytes) forming an aggregate which is occluded as a whole (Figures 2G and 2H; Video S3). In the following studies, we have scrutinized the mechanisms underlying the occlusion-mediated arrest of PGCs.

It is intriguing that whereas PGCs with a diameter of 13.1 ± 1.7 μm are occluded at the constriction point of 9–12 μm width, BCs of a comparable size, which are sporadically seen in the circulation, are not occluded (Figures 2 and S5). We have noticed that this difference is attributed to a deforming ability: PGCs retain their shape, whereas the large BCs easily deform to pass through the constriction point (Figure 2E and Video S3). These observations have raised the possibility that PGCs are highly stiff, enabling efficient occlusion in Ex-VaP.

The circulating PGCs are highly stiff endorsed by cortical actin

To test whether PGCs are stiff, the AFM indentation assay has been conducted to measure the stiffness of a single PGC prepared by harvesting the blood from HH15 chicken embryos (Figure 3A).[11,12] The center of each cell is indented with a spherical bead (10 μm diameter) attached to the tip of a cantilever. The elastic (Young's) modulus obtained by vertical 1 μm indentation on a single PGC is four times higher than that of a BC (Figures 3B, S6, and S7), indicating that PGCs are significantly stiff. Because BCs less than 10 μm of diameter (Figure S5) are indented by 1 μm depth, the bottom effect (rigid underling substrate effect) might occur.[13,14] The bottom effect is known to yield a value stiffer than the actual, meaning that the actual stiffness of BCs might be lower than the obtained value. Collectively, PGCs are highly stiffer than BCs. The values of PGCs' stiffness show bimodal distributions (around 700 Pa and 900 Pa) (Figure 3B), suggesting that circulating population exhibits heterogeneity in their stiffness. For the AFM indentation assay, live PGCs are used, which are easily distinguished morphologically from other BCs and confirmed afterward by marker staining with DDX4 and Phalloidin (Figure 3C, see also below).

Regarding factor(s) endowing PGCs with high stiffness, cytoskeletal components including actin fibers and microtubules are strong candidates.[15–17] Phalloidin staining reveals dense actin fibers distributed beneath the cortical membrane of PGCs, and the signal intensity in PGCs is five times higher than that in BCs (Figures 3C and S8A). In contrast, α-tubulin amounts and its distribution patterns are comparable between PGCs and BCs (Figure S8B).
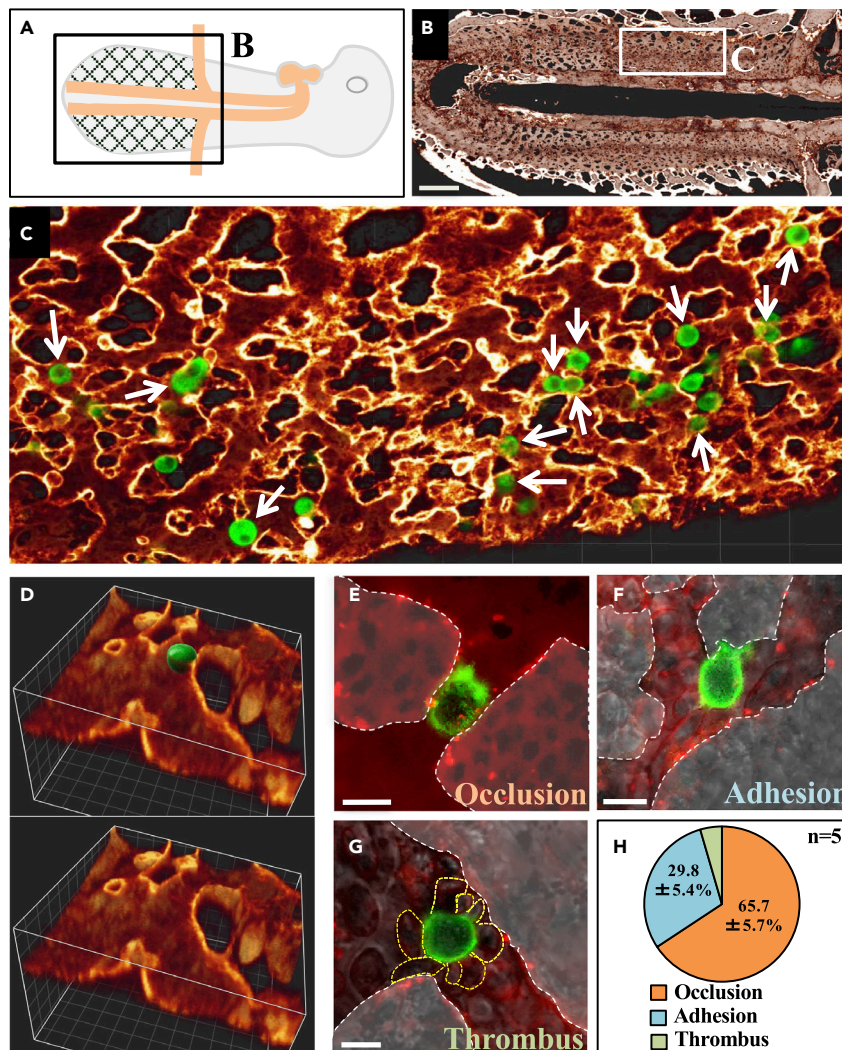
Figure 2. PGCs are occluded at constriction points in Ex-VaP

(A and B) 3D reconstitution of QH1 signal in HH15 quail embryo corresponding to the square in A.

(C) Sliced and magnified view of the square in B. PGCs were labeled by DDX4 immunofluorescence (green). White arrows indicate occluded PGCs in Ex-VaP.

(D) 3D reconstitution image of an occluded PGC and endothelial linings of Ex-VaP. PGC images were reprocessed to 3D iso-surface (green color with texture), and volume images of the endothelial linings (orange) were clipped with appropriate plane.

(E–G) Motion captures taken from Video S3 show occluded, adhered, and thrombus-like PGCs in Ex-VaP at high resolution. PGCs were labeled by TL-conjugated FITC. White and yellow dotted lines delineate the outline of endothelial linings and blood cells attached to the PGC, respectively.

(H) Relative representation of three types of arrests in Ex-VaP, the occlusion, adhesion, and thrombus-like. Each value is a percentage to the total number of arrested PGCs in Ex-VaP of HH15 living embryos (n = 5). Data were extracted from 15-min movies after TL-conjugated FITC infusion. Scale bars: 300 μm in B, 10 μm in E–G. Please see also Figures S3–S5 and Video S3.

To examine whether F-actin function is responsible for the PGC stiffness, actin inhibitors, latrunculin A (inhibiting actin polymerization) or blebbistatin (inhibiting acto-myosin function), have been added to cultured PGCs prepared from HH15 embryos. After 30 min, treated PGCs exhibit drastic reduction in cell stiffness revealed by the AFM assay (Figures 3D and S9). To further trace the F-actin-inhibited PGCs for a prolonged period of time, cultured PGC are gene-manipulated with dominant-negative type of RhoA (DN-RhoA),[18] botulinum C3 enzyme (C3),[18] or β-actin with a point mutation (R62D)[19] known to act as a dominant negative effector against actin polymerization. Each of these genes is Tet-on inducibly expressed in PGCs with Dox administration so that the actin
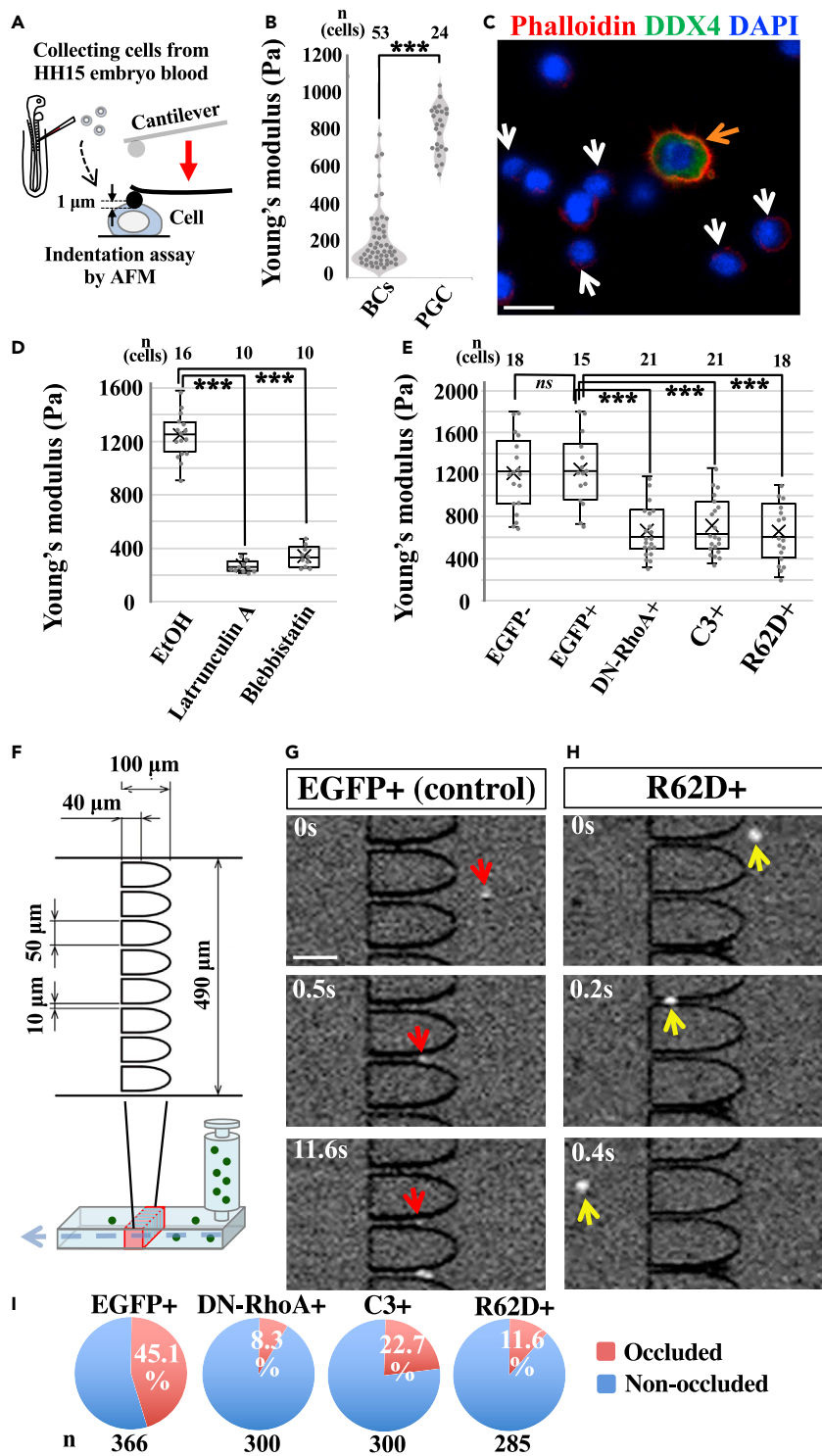
Figure 3. Actin-dependent stiffness of PGCs and occlusion assay

(A) AFM indentation measurement applied to PGCs and blood cells (BCs) harvested from embryonic blood. Living cells attached to the dish bottom are pressed for 1 μm by a cantilever with a bead.

(B) Quantification of cell stiffness measured by AFM indentation tests.

(C) Immunofluorescence of DDX4 (green) and phalloidin staining (red) for PGCs (orange arrow) and BCs (white arrows).

(D) Cell stiffness of EtOH (control)- and chemical reagent-treated PGCs from HH15 chicken embryos.

Figure 3. *Continued*

(E) Cell stiffness of gene-manipulated PGCs. EGFP(+) and EGFP(−) are with and without Dox.

(F) Experimental design with a microfluidic device.

(G and H) Motion captures at indicated timepoints from Videos S4 and S7. A single PGC (red or white arrows) that flows from the right side passes through a slit after remaining at the slit for certain duration of time.

(I) Relative representation of occluded and non-occluded PGCs in the microfluidic constriction assay. Analyzed cell numbers are as indicated from 3 independent experiments. ns, not significant. ***p < 0.001. Scale bars: 10 μm in C, 50 μm in G. Please see also Figures S5–S11 and Videos S4, S5, S6, and S7.

inhibition commences upon the AFM assay but not during the *in vitro* culture for PGC propagation.[20] PGCs treated with each of these three inhibitors have reduced cell stiffness, whereas EGFP-manipulation shows no effect (Figure 3E). Thus, F-actin functions, but not those of microtubules, are necessary for endowing PGCs with stiffness. The cell diameter and the shape of PGCs are not affected by these inhibitors (Figures S5 and S10).

To know whether the cell stiffness plays a major role in the occlusion of PGCs at a constriction point, we have prepared a microfluidic device with multiple micro-slits of 10 μm width and 50 μm height for each (Figure 3F), which is equivalent with the narrowest width among vascular paths in Ex-VaP (Figures 2 and S4). PGCs transfected with Tet-on inducible DN-RhoA, C3, or R62D are streamed into this device at flow velocity of 150–500 μm/s. The surface of the micro-slits has a low cell affinity due to hydrophobic property of dimethylpolysiloxane (PDMS), minimizing the effect on cell adhesion. In this assay, the occlusion is defined as follows: if cells remain at the micro-slit for longer than 5 s, they are regarded as occluded. In contrast, if cells pass through the slit within 5 s, they are regarded as non-occluded. Tet-on EGFP-transfected PGCs (control) are efficiently occluded (45.1%) (Figures 3G and 3I; Video S4). In contrast, most of DN-RhoA-, C3-, or R62D-transfected PGCs are non-occluded (8.3%, 22.7%, and 11.6%, respectively) (Figures 3H, 3I, and S11; Videos S5, S6, and S7). These data indicate that the actin-mediated stiffness is essential for the PGCs' occlusion in a narrow path.

Actin-mediated stiffness of PGCs is critical for the intravascular arrest

To determine whether the actin-mediated stiffness is also crucial for PGCs' occlusion/arrest in Ex-VaP *in vivo*, the aforementioned F-actin-inhibited PGCs (1,000 cells) are infused into host HH15 embryos. Tet-on inducible EGFP-PGCs 9 (control) display normal patterns of arresting rate (40.8% compared to Figure 1G), total arrests in Ex-VaP (65.2 ± 15.7 cells in Ex-VaP), and migration/homing to gonads (82.0 ± 9.5 cells/gonads) comparable with those for TL-labeled- and CAGGS:EGFP-PGCs (Figures 4A, 4C, 4D, 4F, 4G, 4I, 4J, and S12; Video S8), confirming that the Tet-on system does not compromise normal behavior of PGCs *in vivo*. Dox is administered upon the infusion of the gene-manipulated PGCs so that the actin inhibition commences at this time point. Live-imaging analyses reveal that expression of DN-RhoA, C3, or R62D markedly reduces both the arresting rate (6.1%, 8.2%, and 3.2%, respectively) (Figures 4B, 4C, and S13; Videos S9, S10, and S11) and the total number of arrested PGCs in Ex-VaP (10.8 ± 6.2, 28.0 ± 9.3, and 17.8 ± 8.5, respectively) (Figures 4E, 4F, and S14). Importantly, the infused embryos show a significant failure of PGCs both to migrate in the mesentery and to home gonads examined in E4.5 embryos (16.2 ± 10.2, 27.8 ± 14.6, and 30.3 ± 17.4 cells in gonads, respectively) (Figures 4H, 4I, 4J, S12, and S15). Collectively, the F-actin-mediated stiffness is a crucial base for the PGCs to implement the efficient arrest in Ex-VaP, the prerequisite and essential step for the subsequent transmigration across the endothelial lining and migration/homing to gonads (Figure 4L).

PGCs reset its stiffness for transmigration

Following the PGC's arrest in Ex-VaP, they complete the transmigration through the endothelial cell barrier in 1 h (Figure 4K). At this step, the PGCs deform drastically in order to squeeze themselves to pass through an interendothelial space (hole), suggesting that the cell stiffness is quickly reset to soften the cell (Figure 4L). Indeed, when polystyrene beads of 15 μm diameter are infused into a host embryo in a similar way to the PGC experiment, they are successfully arrested at the constriction points in Ex-VaP, but they never transmigrate (Figure S16).

DISCUSSION

We have demonstrated that circulating PGCs are highly stiff, and this stiffness enables the cells to be efficiently occluded at a specific site in Ex-VaP. This occlusion is a prerequisite step for the transmigration of PGCs leading to a successful homing to the gonadal primordium. PGC's stiffness is mediated by cortical actin, dysfunction of which causes a failure of PGC's occlusion resulting in poor homing to the developing gonad. Of note, the PGCs' stiffness is highly dynamic; following the occlusion, the cells immediately reset the stiffness in order to squeeze themselves through a tiny hole of endothelial lining.
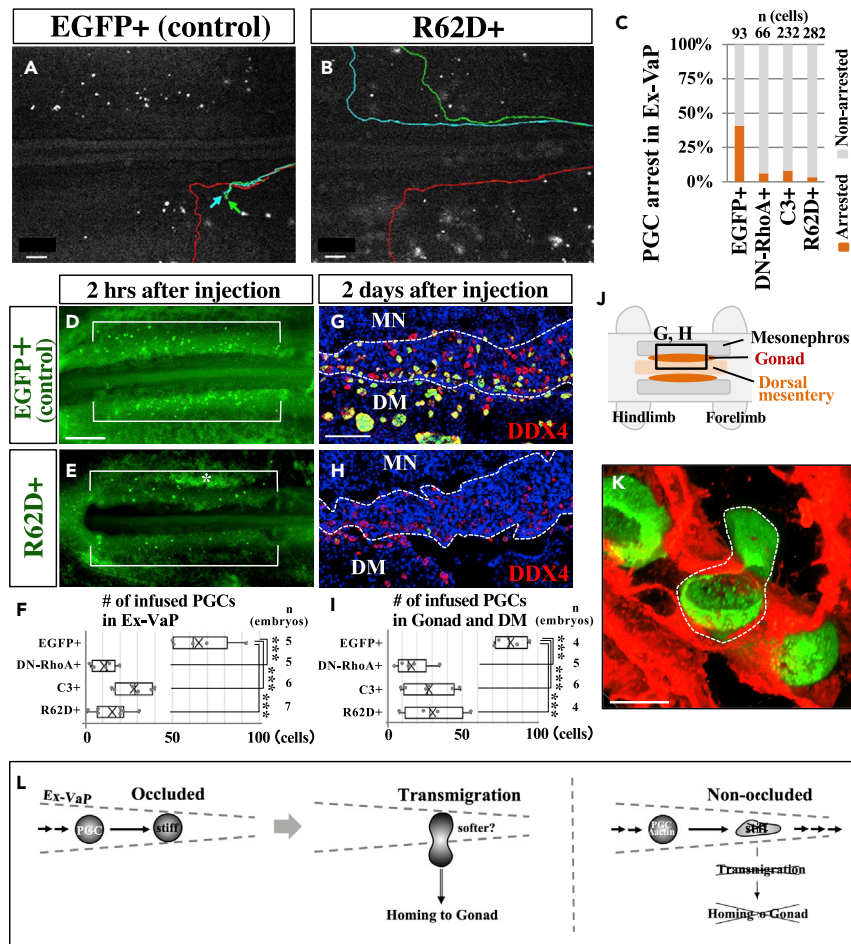
Figure 4. Actin-dependent stiffness of PGCs for the intravascular arrest, and its rapid reset for transmigration

(A and B) Movie captures taken from Videos S8 and S11. Colored lines show tracks of intravascular translocations of PGCs in embryos. Arrows indicate an arrested PGC in Ex-VaP.

(C) Ratio of the arrest of actin-compromised PGCs in Ex-VaP. Analyzed cell numbers are as indicated from 5 embryos.

(D and E) Localization of back-infused PGCs (EGFP-labeled). EGFP immunofluorescence pictures in Ex-VaP (brackets) of HH15 embryos 2 h after infusion with EGFP + or R62D + PGCs. Asterisk shows noise signal.

(F) Quantification of arrested PGCs in Ex-VaP 2 h after infusion with 1,000 PGCs.

(G and H) DDX4 (red) and EGFP (green) immunofluorescence in horizontal sections of E4.5 chicken embryos (HH25) 2 days after infusion with EGFP- or R62D-transfected PGCs. Images correspond to a square in J. Dotted lines delineate the gonad primordium. MN, mesonephros; DM, dorsal mesentery.

(I) Quantification of infused PGCs in the gonads and DM.

(J) Ventral view of HH25 embryo.

(K) 3D reconstitution image of QH1 (red) and DDX4 (green) immunofluorescence of Ex-VaP in HH15 quail embryo. A squeezed PGC enclosed by a white dotted line in the course of transmigration through an inter-endothelial small hole in Ex-VaP.

(L) Summary diagram. Intravascularly circulating PGCs are highly stiff and successfully occluded at a constriction point in Ex-VaP. Subsequently, the occluded PGCs rapidly reset its stiffness to soften in order to squeeze themselves and transmigrate through an endothelial lining. The stiffness of PGCs is mediated by F-actin: F-actin-dysregulated PGCs are much softer, and fail to be occluded in Ex-VaP, resulting in poor colonization in the forming gonad. ***$p < 0.001$. Scale bars: 200 μm in A, B, 500 μm in D, 100 μm in G, 10 μm in K. Please see also Figures S12–S16 and Videos S8, S9, S10, and S11.

PGCs' stiffness is endorsed by cortical actin

PGCs exhibit prominent cortical actin, which endows the cells with high stiffness. F-actin-compromised PGCs are not successfully occluded at micro-slits in the microfluidic assay. More importantly, these cells, when back-infused to embryos, fail to be arrested in Ex-VaP and flow away to an extraembryonic region, causing poor extravasation and homing to the gonadal primordium.

The regulation of actin-mediated stiffness of PGCs must be highly dynamic, since when they start the transmigration through an epithelial lining, the cells reset the stiffness and deform drastically both plasma membrane and nucleus (Figure 4K). Such deformation is often associated with cell blebbing, which is not seen in the circulating PGCs. We previously reported that PGCs at earlier stages prior to circulation also exhibit blebbing.[6] It is known that the blebbing of plasma membrane is not accompanied by underlying cortical F-actin.[21] Therefore, it is likely that the blebbing PGCs are much softer than the circulating PGCs. What assures the stiffness of the circulating PGCs? It has been reported that shear stress by blood flow promotes F-actin stress fiber formation in endothelial cells.[22] Such shear stress might also contribute to PGC's stiffness. For the reset of stiffness, interactions between occluded PGCs and endothelial lining and/or locally changed fluid pressure at the occluded point are conceivable. Alternatively, CXCL12, known to act as a chemoattractant for the homing of PGCs widely in zebrafish,[23] might influence the transmigration of occluded/arrested PGCs in Ex-VaP. CXCL12 is indeed expressed in the splanchnic mesoderm. For the stiff PGCs of 13 μm diameter to be correctly occluded in Ex-VaP, constriction points of 10 μm width are important. It has yet to be studied whether other vasculatures, for example, cephalic capillaries, containing comparable constriction points also trap circulating PGCs.

PGCs extravasation provides a model for the understanding of metastasizing cancer cells

Our findings obtained in this study highlight the possibility that other types of extravasating cells such as metastasizing cancer cells, which are mainly arrested by occlusion in capillary beds,[24–27] might also be highly stiff. Indeed, the "mechanical trap theory" was proposed by James Ewing in 1928, which tried to explain the intravascular arrest of cancer cells.[28] However, since cancer cells *before* the intravascular circulation are not stiffer or even softer than normal cells,[29,30] it remained unexplored whether these cells become stiffer at the time of their arrest in the capillary bed.

It is increasingly appreciated that cancer cells and avian PGCs share common features regarding metabolism and gene expression profiles.[31–36] Avian PGCs, which can be studied at high resolution in a flat structure of an early embryo, serve as a powerful model to decipher the cancer metastasis.

Limitations of the study

1) Currently, a direct measurement of circulating or transmigrating PGCs by AFM *in vivo* is unavailable. To overcome the issues described below, *in vivo* imaging experiments using tension sensor probes must be helpful.

   - Some of PGCs in Ex-VaP escape from constriction points and flow away toward the extraembryonic region. It remains unclear if these cells do so because they are not sufficiently stiff.

   - The transmigrating PGCs must be softer than the occluded PGCs since they drastically deform both the plasma membrane and nucleus. Quantitative measurement of such dynamics is awaited.

2) It remains unknown how the three types of arrest (occlusion type, adhesion type, and thromboid type) are regulated.

STAR★METHODS

Detailed methods are provided in the online version of this paper and include the following:

- KEY RESOURCES TABLE
- RESOURCE AVAILABILITY
  - Lead contact
  - Materials availability
  - Data and code availability
- EXPERIMENTAL MODEL AND SUBJECT DETAILS
  - Animal ethics statement
  - Establishment and maintenance of PGC line
- METHOD DETAILS
  - Animals, staging, and animal care
  - Plasmid constructions
  - Plasmid transfection and establishment of gene-manipulated PGC lines
  - Immunofluorescence staining and phalloidin staining
  - AFM indentation measurement and chemical treatments

- ○ TL-injection, PGC- and bead infusion, Dox administration, and embryo culture
- ○ Microfluidic devices for cell arrest assay
- ○ Capture and process of images
- ● QUANTIFICATION AND STATISTICAL ANALYSIS

AUTHOR CONTRIBUTIONS

D. S. designed the study. D. S. and K. M. performed embryonic manipulations. A. N., M. T., and D. S. performed and analyzed AFM experiments. R. T., H. K., T. T., and D. S. performed imaging experiments. D. Y. and K. F. designed microfluidic device, and D. S. performed the experiments and analyzed data. D. S., K. T., and Y. T. supervised the study. D. S. and Y. T. wrote the manuscript.

DECLARATION OF INTERESTS

The authors declare no competing interests.

REFERENCES

1. Molyneaux, K., and Wylie, C. (2004). Primordial germ cell migration. Int. J. Dev. Biol. 48, 537–544.

2. Richardson, B.E., and Lehmann, R. (2010). Mechanisms guiding primordial germ cell migration: strategies from different organisms. Nat. Rev. Mol. Cell Biol. 11, 37–49.

3. Pierce, J.L., Frazier, A.L., and Amatruda, J.F. (2018). Pediatric germ cell tumors: a developmental perspective. Adv. Urol. 2018, 9059382.

4. Swift, C.H. (1914). Origin and early history of the primordial germ-cells in the chick. Am. J. Anat. 15, 483–516.

5. Nakamura, Y., Yamamoto, Y., Usui, F., Mushika, T., Ono, T., Setioko, A.R., Takeda, K., Nirasawa, K., Kagami, H., and Tagami, T. (2007). Migration and proliferation of primordial germ cells in the early chicken embryo. Poult. Sci. 86, 2182–2193.

6. Murai, H., Shibuya, M., Kishita, R., Sunase, C., Tamura, K., and Saito, D. (2021). Envelopment by endothelial cells initiates translocation of avian primordial germ cell into vascular tissue. Dev. Dyn. 250, 1410–1419.

7. Hamburger, V., and Hamilton, H.L. (1951). A series of normal stages in the development of the chick embryo. J. Morphol. 88, 49–92.

8. Ando, Y., and Fujimoto, T. (1983). Ultrastructural evidence that chick primordial germ-cells leave the blood-vascular system prior to migrating to the gonadal anlagen. Dev. Growth Differ. 25, 345–352.

9. Sato, Y., Kasai, T., Nakagawa, S., Tanabe, K., Watanabe, T., Kawakami, K., and Takahashi, Y. (2007). Stable integration and conditional expression of electroporated transgenes in chicken embryos. Dev. Biol. 305, 616–624.

10. Whyte, J., Glover, J.D., Woodcock, M., Brzeszczynska, J., Taylor, L., Sherman, A., Kaiser, P., and McGrew, M.J. (2015). FGF, insulin, and SMAD signaling cooperate for avian primordial germ cell self-renewal. Stem Cell Rep. 5, 1171–1182.

11. Nagasaka, A., Shinoda, T., Kawaue, T., Suzuki, M., Nagayama, K., Matsumoto, T., Ueno, N., Kawaguchi, A., and Miyata, T. (2016). Differences in the mechanical properties of the developing cerebral cortical proliferative zone between mice and ferrets at both the tissue and single-cell levels. Front. Cell Dev. Biol. 4, 139.

12. Nagasaka, A., and Miyata, T. (2021). Comparison of the mechanical properties between the convex and concave inner/apical surfaces of the developing cerebrum. Front. Cell Dev. Biol. 9, 702068.

13. Dimitriadis, E.K., Horkay, F., Maresca, J., Kachar, B., and Chadwick, R.S. (2002). Determination of elastic moduli of thin layers of soft material using the atomic force microscope. Biophys. J. 82, 2798–2810.

14. Chiodini, S., Ruiz-Rincón, S., Garcia, P.D., Martin, S., Kettelhoit, K., Armenia, I., Werz, D.B., and Cea, P. (2020). Bottom effect in atomic force microscopy nanomechanics. Small 16, e2000269.

15. Naumanen, P., Lappalainen, P., and Hotulainen, P. (2008). Mechanisms of actin stress fibre assembly. J. Microsc. 231, 446–454.

16. Wang, N., and Stamenović, D. (2000). Contribution of intermediate filaments to cell stiffness, stiffening, and growth. Am. J. Physiol. Cell Physiol. 279, C188–C194.

17. Grady, M.E., Composto, R.J., and Eckmann, D.M. (2016). Cell elasticity with altered cytoskeletal architectures across multiple cell types. J. Mech. Behav. Biomed. Mater. 61, 197–207.

18. Tadokoro, R., Murai, H., Sakai, K.I., Okui, T., Yokota, Y., and Takahashi, Y. (2016). Melanosome transfer to keratinocyte in the chicken embryonic skin is mediated by vesicle release associated with Rho-regulated membrane blebbing. Sci. Rep. 6, 38277.

19. Posern, G., Sotiropoulos, A., and Treisman, R. (2002). Mutant actins demonstrate a role for unpolymerized actin in control of transcription by serum response factor. Mol. Biol. Cell 13, 4167–4178.

20. Watanabe, T., Saito, D., Tanabe, K., Suetsugu, R., Nakaya, Y., Nakagawa, S., and Takahashi, Y. (2007). Tet-on inducible system combined with in ovo electroporation dissects multiple roles of genes in somitogenesis of chicken embryos. Dev. Biol. 305, 625–636.

21. Aoki, K., Maeda, F., Nagasako, T., Mochizuki, Y., Uchida, S., and Ikenouchi, J. (2016). A RhoA and Rnd3 cycle regulates actin reassembly during membrane blebbing. Proc. Natl. Acad. Sci. USA 113, E1863–E1871.

22. Kataoka, N., Ujita, S., and Sato, M. (1998). Effect of flow direction on the morphological responses of cultured bovine aortic endothelial cells. Med. Biol. Eng. Comput. 36, 122–128.

23. Doitsidou, M., Reichman-Fried, M., Stebler, J., Köprunner, M., Dörries, J., Meyer, D., Esguerra, C.V., Leung, T., and Raz, E. (2002). Guidance of primordial germ cell migration by the chemokine SDF-1. Cell 111, 647–659.

24. Chambers, A.F., Groom, A.C., and MacDonald, I.C. (2002). Dissemination and growth of cancer cells in metastatic sites. Nat. Rev. Cancer 2, 563–572.

25. Azevedo, A.S., Follain, G., Patthabhiraman, S., Harlepp, S., and Goetz, J.G. (2015). Metastasis of circulating tumor cells: favorable soil or suitable biomechanics, or both? Cell Adh. Migr. 9, 345–356.

26. Katt, M.E., Wong, A.D., and Searson, P.C. (2018). Dissemination from a solid tumor: examining the multiple parallel pathways. Trends Cancer 4, 20–37.

27. Cheng, X., and Cheng, K. (2021). Visualizing cancer extravasation: from mechanistic studies to drug development. Cancer Metastasis Rev. 40, 71–88.

28. Ewing, J. (1928). Neoplastic Diseases. A Treatise on Tumors (W. B. Saunders Co.).

29. Katira, P., Bonnecaze, R.T., and Zaman, M.H. (2013). Modeling the mechanics of cancer: effect of changes in cellular and extra-cellular mechanical properties. Front. Oncol. 3, 145.

30. Suresh, S. (2007). Biomechanics and biophysics of cancer cells. Acta Biomater. 3, 413–438.

31. Whitehurst, A.W. (2014). Cause and consequence of cancer/testis antigen activation in cancer. Annu. Rev. Pharmacol. Toxicol. 54, 251–272.

32. Li, Y., Li, J., Wang, Y., Zhang, Y., Chu, J., Sun, C., Fu, Z., Huang, Y., Zhang, H., Yuan, H., and Yin, Y. (2017). Roles of cancer/testis antigens (CTAs) in breast cancer. Cancer Lett. 399, 64–73.

33. Janic, A., Mendizabal, L., Llamazares, S., Rossell, D., and Gonzalez, C. (2010). Ectopic expression of germline genes drives malignant brain tumor growth in Drosophila. Science 330, 1824–1827.

34. Hayashi, Y., Otsuka, K., Ebina, M., Igarashi, K., Takehara, A., Matsumoto, M., Kanai, A., Igarashi, K., Soga, T., and Matsui, Y. (2017). Distinct requirements for energy metabolism in mouse primordial germ cells and their reprogramming to embryonic germ cells. Proc. Natl. Acad. Sci. USA 114, 8289–8294.

35. Deshmukh, A., Deshpande, K., Arfuso, F., Newsholme, P., and Dharmarajan, A. (2016). Cancer stem cell metabolism: a potential target for cancer therapy. Mol. Cancer 15, 69.

36. Bose, S., and Le, A. (2018). Glucose metabolism in cancer. Adv. Exp. Med. Biol. 1063, 3–12.

37. Chen, Y.C., Lin, S.P., Chang, Y.Y., Chang, W.P., Wei, L.Y., Liu, H.C., Huang, J.F., Pain, B., and Wu, S.C. (2019). In vitro culture and characterization of duck primordial germ cells. Poult. Sci. 98, 1820–1832.

38. Kawakami, K. (2005). Transposon tools and methods in zebrafish. Dev. Dyn. 234, 244–254.

39. Hutter, J.L., and Bechhoefer, J. (1993). Calibration of atomic-force microscope tips. Rev. Sci. Instrum. 64, 1868–1873.

40. Hertz, H. (1881). Über die Berührung fester elastischer Körper. J. für die Reine Angewandte Math. (Crelle's J.) 92, 156–171.

41. Kidokoro, H., Yonei-Tamura, S., Tamura, K., Schoenwolf, G.C., and Saijoh, Y. (2018). The heart tube forms and elongates through dynamic cell rearrangement coordinated with foregut extension. Development 145, dev152488.

STAR★METHODS

KEY RESOURCES TABLE

REAGENT or RESOURCE	SOURCE	IDENTIFIER
Antibodies		
Anti-chicken DDX4	Custom-made	N/A
Anti-α-Tubulin	Sigma-Aldrich	Cat# T6199 RRID: AB_477583
QH1	Developmental Studies Hybridoma Bank	RRID: AB_531829
Anti-EGFP	Abcam	Cat# 6673 RRID: AB_305643
Alexa Fluor 488; Goat anti-rabbit	Thermo Fisher, Invitrogen	Cat# A11034 RRID: AB_2576217
Alexa Fluor 488; Goat anti-mouse	Thermo Fisher, Invitrogen	Cat# A28175 RRID: AB_2536161
Alexa Fluor 555; Donkey anti-rabbit	Thermo Fisher, Invitrogen	Cat# A31572 RRID: AB_162543
Alexa Fluor 488; Donkey anti-goat	Thermo Fisher, Invitrogen	Cat# A11055 RRID: AB_2534102
Chemicals, peptides, and recombinant proteins		
Puromycin	InvivoGen	Cat# ant-pr; CAS# 58-58-2
Poly-L-Lysine	Sigma-Aldrich	Cat# P8920; CAS# 25988-63-0
Poly-ethylenimine	Sigma-Aldrich	Cat# 03880; CAS# 9002-98-6
Latrunculin A	Cayman Chemical	Cat# 10010630; CAS# 76343-93-6
(S)-(−)-Blebbistatin	Toronto Research Chemicals	Cat# B592500; CAS# 856925-71-8
Tomato lectin (TL)-conjugated FITC	Sigma-Aldrich	Cat# L0401
CellMask™ orange plasma membrane stains	Thermo Fisher, Invitrogen	Cat# C10045
Doxycycline	Clontech	Cat# 631311; CAS# 24390-14-5
FluoSpheres™ Polystyrene Microspheres	Thermo Fisher, Invitrogen	Cat# F8841
Alexa Fluor 647 Phalloidin	Thermo Fisher, Invitrogen	Cat# A22287 RRID:AB_2620155
Activin A	Peprotech	Cat# 120-14E
FGFC	FUJIFILM Wako	Cat# 067-06591
Chicken serum	Biowest	Cat# S0500
Critical commercial assays		
Neon™ Transfection System	Thermo Fisher, Invitrogen	Cat# MPK5000S
Recombinant DNA		
pT2A-CAGGS-EGFP	This paper	N/A
pCAGGS-T2TP	Sato et al. (2007)	N/A
pT2A-BI-TRE-EGFP	This paper	N/A
pT2A-CAGGS-Tet3G-2A-PuroR	Tadokoro et al. (2016)	N/A
pT2A-BI-TRE-EGFP-DN-RhoA	This paper	N/A
pT2A-BI-TRE-EGFP-C3	This paper	N/A
pT2A-BI-TRE-EGFP-R62D	This paper	N/A
Software and algorithms		
FIJI-ImageJ	NIH	https://imagej.net/software/fiji/
JPK DP software v.5	JPK Instruments	https://www.nanophys.kth.se/ nanolab/afm/jpk/manuf-manuals/DPmanual.4.2.pdf
Huygens	Scientific Volume Imaging	https://svi.nl/HomePage
Imaris ver.9.5	Oxford Instruments	https://imaris.oxinst.com

RESOURCE AVAILABILITY

Lead contact

Further information and requests for resources and reagents should be directed to and will be fulfilled by the lead contact, Daisuke Saito: saito.daisuke.036@m.kyushu-u.ac.jp.

Materials availability

All unique/stable reagents generated in this study are available from the lead contact with a completed Material Transfer Agreement.

Data and code availability

All data reported in this paper will be shared by the lead contact upon request.

This paper does not report original code.

Any additional information required to reanalyze the data reported in this paper is available from lead contact upon request.

EXPERIMENTAL MODEL AND SUBJECT DETAILS

Animal ethics statement

All animal experiments were performed with the approval of the Institutional Animal Care and Use Committees at Tohoku University, Kyoto University and Kyushu University (protocol #A19-235-0).

Establishment and maintenance of PGC line

Circulating PGCs along with blood cells were harvested from blood of HH 14 female chicken embryo, and were cultured in calcium-free DMEM (Gibco) diluted with water, containing FGF2 (Wako), Activin A (Peprotech), and chicken serum (FAcs medium) according to the method previously described.[10,37] After one month, expanded PGCs were cryo-preserved at −80°C in Bambanker (NIPPON Genetics) until used for experiments.

METHOD DETAILS

Animals, staging, and animal care

Fertilized chicken (*Gallus gallus domesticus*, Hypeco nera) eggs and fertilized quail (*Coturnix japonica*) eggs were purchased from Shiroyama poultry farm (Kanagawa, Japan) and from Nagoya University through the National Bio-Resource Project of the MEXT, Japan, respectively. Eggs were incubated at 38.5°C, and embryos were staged either by the somite number (described as "ss") or by Hamburger and Hamilton's stage.[7]

Plasmid constructions

pT2A-CAGGS-EGFP: pT2AL200R150G vector[38] was digested with XhoI-BglII. This site was blunt-ended, and inserted with the fragment of pCAGGS-EGFP containing the CMV enhancer, βActin promoter, EGFP, and polyA-additional sequences of the rabbit beta globin gene. pT2A-BI-TRE-EGFP: The pT2AL200R150G vector was digested with BglII-XhoI. This site was blunt-ended, and inserted with the fragment of pBI-Tight (Clontech) containing the bidirectional tetracycline-responsive element (TRE) with two minimal promoters of CMV in both directions, and two polyA-additional sequences of the rabbit beta globin gene. This vector was designated as pT2A-BI-TRE. The full-length of EGFP was amplified by PCR, and subcloned into the EcoRI-BglII site of pT2A-BI-TRE. pT2A-BI-TRE-EGFP- (DN-RhoA, C3, or βActinR62D (R62D)): The ORF of a dominant negative form of RhoA (DN-RhoA) or C3 transferase[18] was subcloned into the MluI-EcoRV site of pT2A-BI-TRE-EGFP. The ORF of R62D (kind gift from Drs. Ogura and Kubo)[19] was subcloned into the MluI-NheI site of pT2A-BI-TRE-EGFP. pT2A-CAGGS-Tet3G-2A-PuroR: pT2AL200R150G vector was digested with ApaI-BglII. PCR product including 2A peptide sequence flanking two multi-cloning sites and polyA-additional sequences of the rabbit beta globin gene was ligated into ApaI-BglII site of pT2AL200R150G. This vector was designated as pT2A-MCS1-2A-MCS2. CAGGS promoter sequence was inserted into SalI-PstI site of MCS1 of pT2A-MCS1-2A-MCS2. Tet3G and PuroR PCR products were inserted into the NotI-SphI site of MCS1 and MluI-NheI site of MCS2, respectively.

Plasmid transfection and establishment of gene-manipulated PGC lines

2×10^4 cultured PGCs were washed with OPTI-MEM (Gibco). PGCs were suspended in 10 μL of electroporation re-suspension buffer (R buffer) (Invitrogen). After addition of plasmid DNA (1 μg), they were electroporated by Neon Transfection System (Invitrogen) with optimized condition (1,300 V, 10 ms pulse width, 3 pulses). We used 5 different sets of plasmids (pT2A-CAGGS-EGFP + pCAGGS-T2TP;[9] pT2A-BI-TRE-EGFP + pT2A-CAGGS-Tet3G-2A-PuroR[18] + pCAGGS-T2TP; pT2A-BI-TRE-EGFP-DN-RhoA + pT2A-CAGGS-Tet3G-2A-PuroR + pCAGGS-T2TP; pT2A-BI-TRE-EGFP-C3 + pT2A-CAGGS-Tet3G-2A-PuroR + pCAGGS-T2TP; pT2A-BI-TRE-EGFP-R62D + pT2A-CAGGS-Tet3G-2A-PuroR + pCAGGS-T2TP). Transfected PGCs were seeded into antibiotics-free FAcs medium. After 12 hours, the medium was exchanged to the conventional FAcs medium.

Following pT2A-CAGGS-EGFP transfection, each PGC was separately seeded into 96-well plate dish to obtain EGFP-positive colonies. PGCs receiving the PuroR gene were cultured in the FAcs medium containing 0.5 μg/mL puromycin for two weeks to enrich puromycin-resistant cells.

Immunofluorescence staining and phalloidin staining

For DDX4 and α-Tubulin immunostaining and phalloidin staining in floating PGCs, we mounted living cells with Smear Gell™ (GenoStaff) on an APS-coated slide glass according to the manufacture's instruction. Cells in the slide glass were fixed with 4% PFA/PBS (paraformaldehyde/phosphate buffered saline) for 30 min at room temperature (RT). Specimens were washed in PBS and blocked with 1% blocking reagents (Roche)/TNT (0.1 M Tris-HCl (pH 7.5), 0.15 M NaCl, 0.05% Tween 20) for one hour at RT. The slide glasses were incubated at 4°C overnight with anti-DDX4 rabbit polyclonal antibody (custom-made by Eurofins genomics, 1:10,000), or anti-α-Tubulin antibody (mouse T6199, SIGMA, 1:4,000) in the blocking solution. After 3 washes in TNT for 5 min each, the specimens were reacted with anti-rabbit IgG-Alexa 488-conjugated goat antibody (Invitrogen) diluted 1:1,000 or anti-mouse IgG-Alexa 488-conjugated goat antibody 1:1,000, Alexa Fluor 647 Phalloidin (ThermoFisher, 1:100), and DAPI in blocking solution for one hour at RT. The specimens were washed 3 times in TNT and sealed with FluoSave reagent (Calbiochem).

For immunostainings with DDX4, QH1, and EGFP in whole embryos and dissected gonad/mesonephros, samples were fixed in 4% PFA/PBS for 24 hours at 4°C. They were washed in PBT (PBS with 0.05% Tween 20) three times for 5 min each at RT. They were dehydrated step wise in 25%, 50%, and 75% methanol/PBT (15 min each), followed by incubation in 3% H_2O_2/methanol for 1 hour at RT, and complete dehydration in 100% methanol for 1 hour at RT. They were hydrated step wise in 75%, 50%, and 25% methanol/PBT (15 min each), and then washed with TNTT (0.1 M Tris-HCl (pH 7.5), 0.15 M NaCl, 0.05% Tween 20, 0.1% TritonX-100) (three times 5 min at RT). Blocking was performed in 1% blocking reagents/TNTT for 1 hour at RT. The blocked samples were treated at 4°C overnight with anti-DDX4 rabbit polyclonal antibody (custom-made by Eurofins genomics, 1:2,000), QH1 antibody (Hybridoma Bank, 1:2), and/or anti-EGFP goat polyclonal antibody (goat, abcam, 1:1,000) in the blocking solution. After six 1-hour washes in TNTT at RT, the samples were treated with 1:500 anti-rabbit IgG-Alexa 555-conjugated donkey antibody, 1:500 anti-mouse IgG-Alexa 468-conjugated donkey antibody, and/or 1:500 anti-goat IgG-Alexa 488-conjugated donkey antibody in 1% blocking solution at 4°C overnight. Finally, they were washed six times for 1 hour each in TNTT at RT.

For immunostainings with DDX4, QH1, and EGFP on histological sections, chicken and quail embryos were fixed in 4% PFA/PBS for 24 hours at 4°C. They were washed in PBS for 5 min at RT, and dehydrated by 30% sucrose/PBS at 4°C for 3–6 hours. They were treated with the solution OCT compound (Tissue-Tek) and 30% sucrose/PBS (2:1) at 4°C overnight and embedded in OCT compound. Frozen sections of embedded samples (10 μm thick) were prepared with a cryostat (Microm, HM500 OM). Sections were washed in TNT three times for 5 min, treated with 3% H_2O_2/methanol for 30 min at RT, and washed in TNT three times for 5 min. After 1 hour of blocking with 1% blocking reagents/TNT, the sections were incubated overnight at 4°C with a 1:2,000 dilution of anti-DDX4 rabbit polyclonal antibody, a 1:2 dilution of QH1 antibody, and/or a 1:1,000 dilution of anti-EGFP goat polyclonal antibody. After three 5-min washes in TNT at RT, they were incubated with 1:500 dilution of anti-rabbit IgG-Alexa 555-conjugated donkey antibody, anti-mouse IgG-Alexa 468-conjugated donkey antibody, and/or anti-goat IgG-Alexa 488-conjugated donkey antibody in 1% 1% blocking reagents/TNT for 1 h at RT. After four 5-min washes in TNT at RT, they were sealed by FluorSave reagent (Calbiochem) with DAPI.

AFM indentation measurement and chemical treatments

To attach PGCs or blood cells on a plastic dish, dishes were pre-coated with 0.01% poly-L-lysine solution (SIGMA) or 0.1% poly-ethylenimine (SIGMA) for 30 min at 4°C. After 3 times washes in PBS, cells were seeded in a dish with Dulbecco's modified Eagle medium/Ham's F-12 medium (SIGMA), and incubated for 30 min for 37°C in 5% CO_2. After adding Latrunculin A (Cayman Chemical) or blebbistatin (Toronto Research Chemicals), floating cells were removed.

All measurements were made with Cellhesion200 (JPK Instruments, Berlin, Germany) mounted on an IX71 inverted microscope (Olympus) equipped with a cantilever with a borosilicate bead (sQUBE, CP-CONT-BSG, 10 μm diameter). The spring constant of each cantilever was determined before measurements were made using the thermal noise method[39] in air (nominal value, 0.2 N/m). The applied forces was 1 nN for the dissociated cells and the approach and retraction velocities were 650 nm/s. The indentation depths were ∼1 μm. Each measurement point was set at the top of each dissociated cell. A force-distance curve was analyzed with JPK DP software v.5 (JPK Instruments). Briefly, the Hertz model[40] was applied to calculate Young's modulus as follows:

$$F = \frac{E}{1 - v^2}\left[\frac{a^2 + R^2}{2} \ln\frac{R + a}{R - a} - aR\right]$$

where F is the force, E is the Young's modulus, v is the Poisson's ratio, a is the radius of the contact circle, and R is the radius of sphere. Each cell was measured three times and the mean value was calculated.

TL-injection, PGC- and bead infusion, Dox administration, and embryo culture

Tomato lectin (TL)-conjugated FITC (SIGMA) was diluted by OPTI-MEM (50 μg/mL) for PGC visualization. To visualize both PGCs and blood plasma, CellMask[TM] orange plasma membrane stains (Life Technologies) was added to the TL-FITC working solution at a 1:1,000 dilution. 1 μL of TL-FITC with/without CellMask was injected into the heart of HH15 embryos by a fine glass capillary (Narishige, GD-1) prepared with the puller (Narishige, PC-10).

For back-infusion, cultured PGCs were collected by centrifugation at 100 g for 5 min with several washes in OPTI-MEM. The number of living cells was adjusted to 1,000 cells/μL, and 1 μL of such suspension was injected into the heart of HH15 embryos by a fine glass capillary. For the tet-on induction, 1 μg/mL Doxycycline (Dox) (Clontech) was added into PGC-cultured FAcs medium 12 hours before the injection. Red fluorescent beads of 15 μm diameter (Invitrogen, FluoSpheres[TM] Polystyrene Microspheres) were washed three times in PBS, and suspended in OPTI-MEM. The number of beads was adjusted to 1,000 beads/μL, and 1 μL of such suspension was infused into the heart of HH15 embryos with a glass capillary. For the Tet-on induction *in ovo,* a solution of Dox (0.5 mL of 100 μg/mL) was injected into the egg between the embryo and yolk.[20] For live-imaging, manipulated embryos were removed from eggs using filter paper rings and placed ventral-side down on 35 mm glass bottom dishes, which was pre-coated with thin albumen, or placed ventral-side up on 35 mm plastic culture dishes. containing agarose-albumen medium (0.2% agarose, 50% albumen, 50% saline: 123 mM NaCl in H_2O).[41] They were cultured at 38.5°C.

Microfluidic devices for cell arrest assay

In fabrication of the microfluidic device, the channel pattern with nine 10 μm-slits was transferred from silicon wafer to polydimethylsiloxane mold (PDMS; Silgard 184 Silicone Elastomer Kit, Dow Corning, USA) by soft lithography. Holes for the inlet and outlet with the diameter of 2 mm were punched to access the channel. The patterned side of the PDMS mold and a glass cover slip were bonded with each other after plasma treatment for 1 min and 40 seconds. The channel was filled with sterilized ultrapure water for preservation. In order to provide hydrophobic property to the device, we dried the device at 60°C for 24 hours prior to the experiments.

Dox treated-PGCs suspended in OPTI-MEM (1,000 cells/μL) were loaded in 1 mL syringe (Terumo), and pumped to the microfluidic device at 7 pL/min by syringe pump Legato 110 (KD Scientific).

Capture and process of images

For live imaging, cultured embryos or microfluidic device were set in a humid chamber at 37°C. Movies were taken by a cooled CCD camera, ORCA-R2 (HAMAMATSU Photonics) attached to the macro zoom

microscope MVX10 (Olympus) with the software High Speed Recording (HAMAMATSU Photonics), or A1R confocal microscope (Nikon). Obtained images were processed with Manual Tracking Tool of ImageJ (https://imagej.nih.gov/ij/). For fixed cells and tissue sections, images were obtained with SP5 confocal microscope (Leica). Images of fixed whole samples were obtained with M205 FA stereomicroscope (Leica) or A1R confocal microscope (Nikon). Acquired Z-series images were deconvoluted and processed for 3D reconstruction by using Huygens (Scientific Volume Imaging) and Imaris software (ver.9.5, Oxford Instruments), respectively. Regions of interest (ROIs) showing PGC occlusion in narrow vascular plexus were selected from the whole image. The PGC images were further reconstructed to 3D iso-surfaces with texture, and volume images of plexus structure were clipped with appropriate x-y plane(s).

QUANTIFICATION AND STATISTICAL ANALYSIS

All box plots represent the mean, upper and lower interquartile, error bars (s.e.m) with median (x). p values were obtained by a 2-tailed, unpaired Student's *t* test (Excel). Box plots and bar graphs were made by Excel, and a violin plot was made by RAWGraphs.